J. Fluid Mech. (2000), *vol.* 413, *pp.* 149–180. Printed in the United Kingdom

Slow waves of boiling under hot water depressurization

By OLEG E. IVASHNYOV, MARINA N. IVASHNEVA AND NICKOLAI N. SMIRNOV

Department of Gas and Wave Dynamics, Faculty of Mechanics and Mathematics, Moscow MV Lomonosov State University, Moscow 119899, Russia
e-mail: ebifsun1@mech.math.msu.su

(Received 1 April 1998 and in revised form 28 June 1999)

Experimental studies of hot water depressurization show that the pressure in a vessel, just after it is opened, drops much lower than the pressure of saturation but the liquid does not boil uniformly throughout the vessel. Essentially, liquid boiling begins only on the arrival of a 'slow wave' of rarefaction which moves at a low speed of approximately $10\,\mathrm{m\,s^{-1}}$ from the open end deep into the vessel.

To explain this phenomenon we suggest a model that takes into account the difference in phase velocities. Although this difference in bubble flows is only about $1\,\mathrm{m\,s^{-1}}$ it proves to be sufficient to cause bubble breakup. Using this model we obtained the 'slow wave of boiling' in a numerical experiment that was in good agreement with the physical experiment.

1. Introduction

In a normally working nuclear reactor the hot water is under high pressure. If there is damage water starts to flow out at a high speed. Owing to the drop of pressure this efflux is accompanied by boiling. To create a reactor safety system, it is necessary to understand the properties of such flows, i.e. a model for boiling liquid flows is necessary that could at least qualitatively explain known experiments. The formation of a 'slow wave of boiling' is one of the major characteristics of such flows. The aim of our study was to explain this phenomenon.

The 'slow wave' was first discovered in the experimental results of Edwards & O'Brien (1970) by Labuntsov & Avdeev (1981). Edwards & O'Brien studied the depressurization of a high-pressure vessel, which was a 4 m length tube with 7.3 cm internal diameter. The tube initially contained hot water with temperature $T_0 = 515\,\mathrm{K}$. The pressure in the tube, $P_0 = 6.9$ MPa, was twice the pressure of saturation and the water did not boil. The right-hand end of the tube was closed with a glass disc. On destroying the disc the liquid efflux started. As the atmospheric pressure was less than the pressure of saturation the liquid efflux was accompanied by flashing. Experimental pressure oscillograms measured at five tube cross-sections are shown by solid lines in figures 1(*a*) and 2. At the fourth point the volumetric vapour fraction was additionally measured by an X-ray absorption system (solid line in figure 2*c*).

A uniform pressure of 2.7 MPa, which was less than the pressure of saturation (3.5 MPa), settled at points 3, 4, 5 almost immediately after the vessel opened (i.e. in the short time of 3 ms necessary for a wave moving with the speed of sound in a

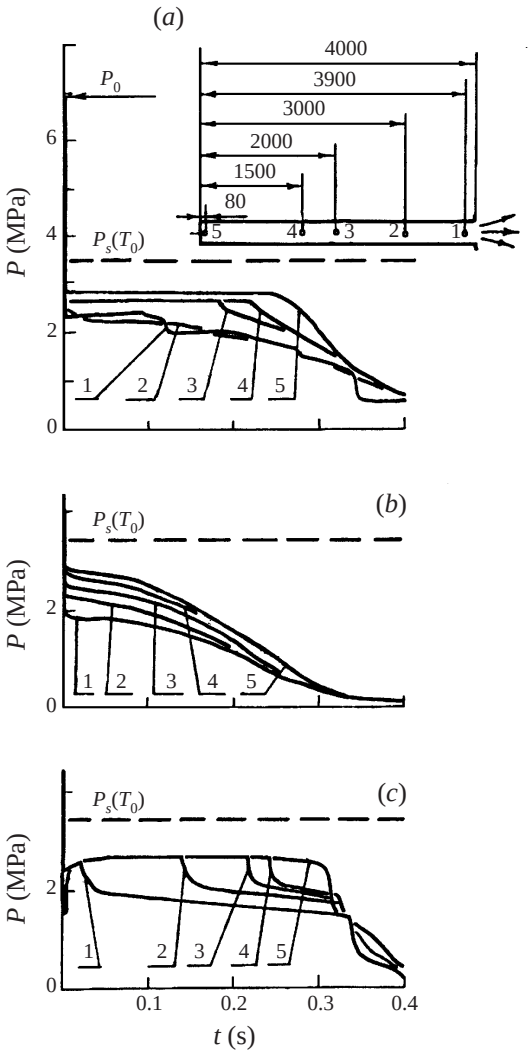

FIGURE 1. Pressure oscillograms at five different tube cross-section locations (shown in the inset): (*a*) the experiment of Edwards & O'Brien (1970); (*b*) calculation with the model of boiling at a constant number of centres (Nigmatulin & Soplenkov 1980); (*c*) calculation with the advanced model accounting for bubble breakup.

pure liquid, $\approx 1000\,\mathrm{m\,s^{-1}}$, to travel the length of the channel). The pressure remained constant for a long time: only after 0.2 s did it start to decrease rapidly at the 3rd point, and then at the 4th and 5th points. This was a 'slow wave' of rarefaction moving with the speed of only $10\,\mathrm{m\,s^{-1}}$ (figure 1*a*). The experimental oscillograms of pressure and volumetric vapour fraction measured at the 4th point clearly showed that the pressure drop in the 'slow wave' was accompanied by a large increase in the volumetric vapour content (solid lines in figure 2*b*, *c*).

An analogous wave configuration had been observed in Edwards & O'Brien's experiments under different initial parameters. Later it was observed by Isaev (1980) when investigating the boiling CO_2 efflux and by Winters & Merte (1979) in experiments with dichlorodifluoromethane (R12).

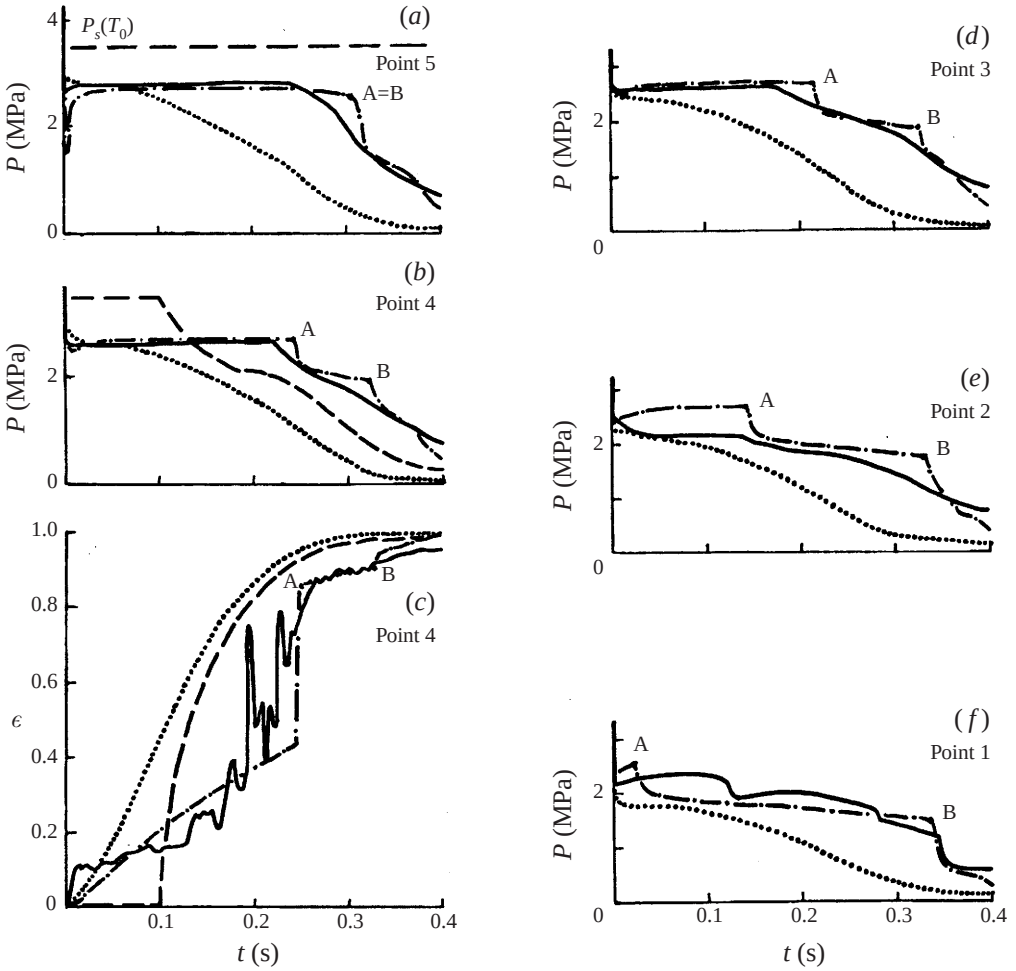

FIGURE 2. A comparison of experimental and theoretical oscillograms of pressure for each of the five tube cross-sections shown in figure 1 and of volumetric vapour content for point 4: ——, experiment; – – –, equilibrium model; ⋯, model of boiling at a constant number of centres; –•–, advanced model accounting for breakup. For a discussion of points A and B see § 6.1.

The known models of liquid boiling cannot explain the 'slow wave' phenomenon.

1.1. *An equilibrium model*

The temperatures, pressures and velocities of the liquid and vapour phases are considered equal in this model. The equilibrium model includes the equations of conservation for mixture mass

$$\frac{\partial \rho}{\partial t} + \frac{\partial}{\partial x}[\rho u] = 0, \tag{1}$$

mixture momentum

$$\frac{\partial}{\partial t}[\rho u] + \frac{\partial}{\partial x}[\rho u^2 + P] = 0, \tag{2}$$

and mixture entropy

$$\frac{\mathrm{d}S}{\mathrm{d}t} = 0, \tag{3}$$

where ρ is the mixture density, u is the flow velocity, P is the pressure, S is the mixture entropy, and

$$\frac{\mathrm{d}(\,)}{\mathrm{d}t} = \frac{\partial(\,)}{\partial t} + u\frac{\partial(\,)}{\partial x}$$

is the substantial derivative.

The equilibrium model contains the equation of state for the medium in the following form:

$$\rho = \rho_L(P, S) \qquad \text{if } P > P_s(T_0), \tag{4a}$$

$$\frac{1}{\rho} = \frac{1}{\rho_L} + \varphi(P)(S - S_L) \quad \text{if } P \leqslant P_s(T_0), \tag{4b}$$

where P_s is the pressure of saturation. Equation (4b) follows from the condition of the equality of liquid and vapour thermodynamic potentials of the components of a boiling mixture.

Here ρ_L is the liquid density,

$$\varphi(P) = \left(\frac{\partial T}{\partial P}\right)_{sat}$$

is the derivative of temperature with respect to pressure on the line of saturation, S_L is the liquid entropy.

It follows from the equation of state (4) that at $P = P_s(T_0)$, the speed of sound

$$a_e^2 = \left(\frac{\partial P}{\partial \rho}\right)_{S=const}$$

changes instantaneously from the speed of sound in a pure liquid, $1100\,\mathrm{m\,s^{-1}}$, down to the speed of sound in an equilibrium two-phase mixture

$$\frac{1}{a_e^2} = \frac{\rho^2}{\rho_L^2 a_L^2} + \rho\left[\left(1 - \frac{\rho}{\rho_L}\right)\frac{1}{\varphi}\left(\frac{\partial^2 T}{\partial P^2}\right)_{sat} - \frac{\rho\varphi}{\rho_L T}\left(\rho_L\left(\frac{\partial i_L}{\partial P}\right)_{sat} - 1\right)\right], \tag{5}$$

which is much less: $a_e = 26\,\mathrm{m\,s^{-1}}$ (at 515 K). In (5) a_L is the speed of sound in the liquid, i_L is the enthalpy of the liquid.

Therefore the wave of rarefaction is split into two waves moving with different velocities. The first wave where the pressure drops down to $P_s(T_0)$ spreads with the speed $1100\,\mathrm{m\,s^{-1}}$. The second wave, where further diminishing of the pressure occurs, moves with the speed $26\,\mathrm{m\,s^{-1}}$. These two waves are separated by a zone of constant pressure $P_s(T_0)$. The calculations using the equilibrium model are shown in figure 2(b, c) by dashed lines. The distribution of pressure at $t = 3\,\mathrm{ms}$ is shown in figure 3 by a dashed line. The two parts of the rarefaction wave are seen.

Thus, according to the equilibrium model the pressure behind the first part of the wave of rarefaction is equal to the pressure of saturation, 3.5 MPa, while in the experiment it is much less, 2.7 MPa (solid lines in figure 2 and circles in figure 3).

1.2. *Models considering thermal non-equilibrium of phases*

Experiments show that in the first rarefaction wave the pressure decreases below the saturation level. Thus, at the first stage of the process the intensity of vaporization is not enough to compensate the drop in the pressure. Apparently the small interphase area cannot provide sufficiently intensive boiling. As a result the pressure drops much lower than the pressure of saturation and the liquid temperature is higher than the

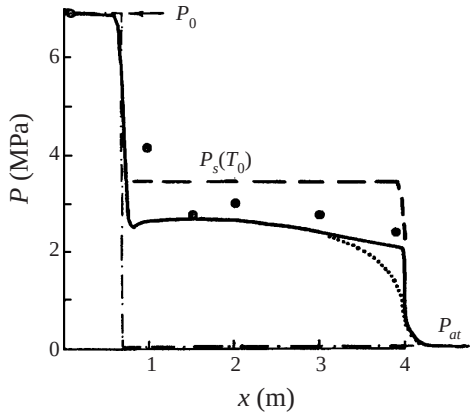

FIGURE 3. The stage of fast waves: the pressure distribution along the channel at $t = 3$ ms. Circles, experiment; –•–, calculations under the assumption that the liquid does not boil; – – –, calculations with the equilibrium model; • • •, calculations with the model of boiling at a constant number of centres; ——, calculation with the advanced model accounting for bubble breakup.

temperature on the line of saturation. One of the models accounting for phase non-equilibrium is the model of boiling at a constant number of nucleation centres of Nigmatulin & Soplenkov (1980). The model considers the pressures and velocities in the liquid and vapour phases to be equal, $P_L = P_G = P, u_L = u_G = u$, but temperatures are considered to be different, $T_L \neq T_G$. The parameters in a bubble are assumed to be uniform and equal to the parameters on the line of saturation. The liquid is assumed to boil only on admixtured particles existing in it, so the number of bubbles per unit mixture mass c remains constant ($c = \text{const}$). The number c is the only free model parameter.

Along with the equations for mixture mass (1) and momentum (2), the model of Nigmatulin & Soplenkov comprises the equation for internal energy

$$\frac{\mathrm{d}i}{\mathrm{d}t} - \frac{1}{\rho}\frac{\mathrm{d}P}{\mathrm{d}t} = 0, \tag{6}$$

and the equation of state for the mixture

$$\frac{1}{a_f^2}\frac{\mathrm{d}P}{\mathrm{d}t} = \frac{\mathrm{d}\rho}{\mathrm{d}t} + J, \tag{7}$$

where $i = (1-\chi)i_L + \chi i_G$ is the mixture enthalpy, i_L, i_G are the enthalpies of the liquid and vapour; $\chi = \rho_G \epsilon/\rho$ is the mass vapour fraction; ρ_G is the vapour density; ϵ is the volumetric vapour fraction; a_f is a 'frozen' speed of sound (the expression for it will be given later);

$$J = jc\rho^2\left(\frac{1}{\rho_G} - \frac{1}{\rho_L}\right); \tag{8}$$

c is the number of bubbles per unit mixture mass; j is the mass of liquid evaporating into one bubble per second. To define j they use a self-similar solution of the problem of the thermal growth of a bubble in an overheated liquid (Scriven 1959). The use of this solution is valid if the time for the temperature profile around the bubble to reach that corresponding to a self-similar solution τ_T is much less than the characteristic time of the process.

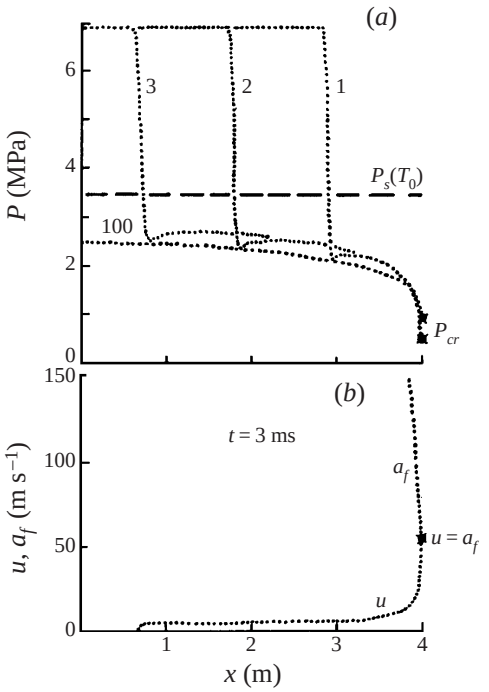

FIGURE 4. Calculation using the model of boiling at a constant number of centres (Nigmatulin & Soplenkov 1980). Numbers next to the curves in (*a*) correspond to time in milliseconds.

The self-similar solution gives the link between the dimensionless temperature gradient at the bubble surface, a Nusselt number

$$Nu = \frac{2a}{T_L - T_s} \left. \frac{\partial T}{\partial r} \right|_{r=a},$$

and a Jacob number

$$Ja = \frac{c_L \rho_L (T_L - T_s)}{\rho_G l}, \tag{9}$$

where a is the bubble radius; $T_s = T_G$ is the temperature of saturation – the temperature at the bubble surface, $T_s = T_s(P)$; c_L is the specific heat capacity of the liquid; l is the specific heat of vaporization.

When $\rho_G \ll \rho_L$, Labuntsov *et al.* (1964) suggested an approximate formula corresponding to the exact solution of Scriven with an accuracy of 2%:

$$Nu = 2 + \left(\frac{6Ja}{\pi} \right)^{1/3} + \frac{12\,Ja}{\pi}. \tag{10}$$

The intensity of liquid evaporation j, expressed via Ja and Nu, has the following form:

$$j = 2\pi D_L \rho_G a\, Ja\, Nu, \tag{11}$$

where $D_L = \lambda_L/(\rho_L c_L)$ is the coefficient of temperature conductivity of the liquid; λ_L is its coefficient of thermal conductivity.

To fit the experimentally measured pressure drop below the saturation one Nigmatulin & Soplenkov (1980) assumed the free model parameter $c = 6 \times 10^5\,\mathrm{kg}^{-1}$. In

fact the free model parameter c can vary for different fluids, and for the same fluid; it depends on its purity.

The results of their calculations are shown in figure 1(*b*) and in figures 2 and 4 by dotted lines. The fact that the pressure in the tube remains much higher than atmospheric pressure for a long time was explained by the effect of the flow 'choking'. After opening the vessel a fast wave of rarefaction moves into the channel (figure 4*a*). Behind the wave the pressure drops below the line of saturation (dashed line) and liquid starts boiling. Vapour generation causes the expansion of the mixture. Due to the expansion the velocity of the flow increases along the channel length. Simultaneously, boiling causes the decrease of the speed of sound. And the velocities become equal at the tube exit (figure 4*b*)

$$u(x = 4\,\mathrm{m}) = a_f.$$

After that the low atmospheric pressure can no longer penetrate into the channel. The pressure in the tube is stabilized at a level that provides an intensity of boiling sufficient to accelerate the flow up to the speed of sound due to the mixture expansion.

But the model of Nigmatulin & Soplenkov (1980) does not predict a 'slow wave' of boiling. The calculations (figure 1*b*) and dotted lines in figure 2 do not show a 'slow wave' in the experiment (solid lines).

Since the complex models could not describe the flows of boiling liquid, Labuntsov & Avdeev (1981) proposed their own simple model – 'a concept of shock boiling'. They postulated that liquid did not boil until the pressure fell to P^* which was less than the pressure of saturation, $P^* < P_s(T_L)$. Below P^*, the liquid started to boil, transforming instantaneously from a metastable liquid to an equilibrium mixture. This transformation occurred in a shock wave of rarefaction. P^* was a free parameter of their model. Calculations for many flows of boiling liquid with the simple model coincided well with the experimental data. However, Labuntsov & Avdeev did not suggest a model of the processes inside a 'slow wave' which could be verified in calculations of the wave structure. Also, the experiment shows that liquid boils before the slow wave arrives (figure 2*c*), in contradiction with their model.

2. Physical model of the process

As we have just seen the model of boiling at a constant number of nucleation centres predicts a more rapid pressure drop than that detected in the experiment. Obviously additional centres of boiling appear during the efflux in the real flow, intensify phase transitions and lead to the pressure growth. The boiling non-uniformity made us give up the hypothesis of uniform birth of additional boiling centres in the flow and we looked instead for a correlation of the formation of additional boiling centres with the hydrodynamic parameters of the flow.

The basic idea of the model we suggest is taking into account the possibility of bubble breakup due to Kelvin–Helmholtz instability of the bubble surface. For bubble breakup a definite correlation between the bubble dimension and the difference in phase velocities must occur. The bubble breakup leads to enlargement of the interface area and boiling intensification. Namely, the bubble breakup takes place in the 'slow wave' and leads to the intensive evaporation in it.

To test this hypothesis we constructed a model to take into account a small difference in phase velocities along with the thermal non-equilibrium of the mixture.

3. The model of boiling liquid flow considering bubble breakup

3.1. *Assumptions and empirical rules*

The model is intended to be applied to fluids below the critical temperature

$$T \leqslant 0.9\, T_{cr}. \tag{12}$$

The critical temperature for water is $T_{cr} = 647\,\mathrm{K}$. Thus the range of model validity for water is $T \leqslant 590\,\mathrm{K}$. The following assumptions are considered.

(i) Homogeneous nucleation, i.e. the formation of boiling centres where the bonds between the liquid molecules break, can be neglected for such 'low' temperatures. The theory of homogeneous nucleation proved experimentally by Scripov and co-workers (Skripov 1972) predicts that the number of bubbles appearing in a unit of volume per unit time can be expressed by the following formula:

$$\psi = \psi_* \exp(-Gi) \tag{13}$$

where ψ_* in the first approximation is considered to be a constant depending on the type of liquid ($\psi_* \sim 10^{38}\,\mathrm{m^{-3}\,s^{-1}}$ for water). Gi is the Gibbs number

$$Gi = \frac{16\pi\sigma^3}{3kT_L(P_s - P_L)^2(1 - \rho_G/\rho_L)^2}. \tag{14}$$

Here σ is surface tension; $k = 1.381 \times 10^{-23}\,\mathrm{J\,K^{-1}}$ is the Boltzmann constant; T_L is the liquid temperature; $P_s - P_L$ is the difference in the pressures in the saturated vapour and in the liquid.

To evaluate the nucleation intensity let us assume the most favourable conditions for intermolecular bond breakup: the liquid at zero pressure and maximal temperature satisfying (12). Under these conditions the rate of nucleation given by (13) is the following:

$$\psi(T_L = 590\,\mathrm{K}, P_L = 0) = 10^{-6}\,\mathrm{m^{-3}\,s^{-1}}.$$

Thus only 10^{-9} bubbles could appear due to homogeneous nucleation within the whole vessel during the time of the process. The probability of intermolecular bond breakup becomes significant only when the coefficient of surface tension is approaching zero, i.e. under the liquid parameters near the critical state: $T \geqslant 0.96\, T_{cr} \approx 620\,\mathrm{K}$.

Thus only heterogeneous nucleation is possible under such 'low' temperatures (12). Therefore we assume that the admixed particles are present in the liquid and when the pressure falls below the saturation value those particles serve as the centres that nucleate boiling. The number of particles per unit mixture mass c_0 is a free model parameter.

(ii) The characteristic time for the pressure to become uniform within a bubble can be evaluated by

$$\tau_{Pb} \sim a^*/a_v,$$

where $a_v \approx 500\,\mathrm{m\,s^{-1}}$ is the speed of sound in a heated vapour; a^* is the typical bubble radius.

For the known superheats of the liquid and the characteristic time of the process τ^*, assuming the pressure to be constant, one can evaluate the typical bubble radius

a^* from the equation for the bubble mass

$$\frac{\mathrm{d}_G m}{\mathrm{d}t} = j, \tag{15}$$

where $m = 4\pi a^3 \rho_G/3$. Equation (15) with the help of (11) can be transformed into the form

$$a\dot{a} = \frac{D_L}{2} Ja\, Nu.$$

The superheats being around 15 K for the process under consideration, the Jacob and Nusselt numbers can be evaluated from (9) and (10) as $Ja \approx 2$; $Nu \approx 10$. Assuming that the characteristic time of the process is $\tau^* \sim 0.1$ s (which follows from experiments: figures 1 and 2), one obtains the following estimate for the bubble radius:

$$a^* \sim \sqrt{D_L\, Ja\, Nu\, \tau^*} \sim 0.1 - 1\,\mathrm{mm}.$$

Therefore:

$$\tau_{Pb} \sim 10^{-6} \ll \tau^*.$$

Thus we can consider the pressure within bubbles to be uniform and equal to the pressure at the fluid–gas interface, i.e. the pressure of saturation:

$$P_G = P_{sat}. \tag{16}$$

The characteristic time for the temperatures to become uniform over all the bubble can be evaluated as

$$\tau_{Tb} \sim (a^*)^2/D_G \sim 1\,\mathrm{s},$$

where

$$D_G = \frac{\lambda_G}{\rho_G c_G} \sim 10^{-6}\,\mathrm{m^{-2}\,s^{-1}}$$

is the coefficient of temperature conductivity of vapour.

Though the characteristic time τ_{Tb} is much larger than the characteristic time of the process, we nevertheless assume the temperature in a bubble to be uniform:

$$T_G = T_s. \tag{17}$$

Thus distorting the actual temperature profile in a bubble, we introduce an error in determining the heat flux from the vapour to the bubble surface

$$q_G = 4\pi a^2 \lambda_G \left.\frac{\partial T}{\partial r}\right|_{r=a}.$$

However the heat flux from vapour to the bubble's boundary is much less than the heat flux from the liquid,

$$q_G \ll q_L = 4\pi a^2 \lambda_L \left.\frac{\partial T}{\partial r}\right|_{r=a},$$

since $\lambda_G \sim 0.1\lambda_L$ in our range of temperatures. Therefore the error in the q_G definition does not in practice influence the accuracy of determining the intensity of evaporation into a bubble. Thus the assumption (17) is quite reasonable and the vapour in the bubbles can be considered to be in the state of saturation.

(iii) An air bubble can oscillate in fluid for a relatively long time until pressures in the bubble and surrounding fluid reach an equilibrium. But in the case of intensive

evaporation it was shown (Nigmatulin 1987) that bubble oscillations decrease rapidly and in 2 or 3 pulsations pressures in the phases almost reach an equilibrium. The characteristic time for equalizing the pressures in the phases can be evaluated by

$$\tau_{PP} \sim (2-3)a^* \sqrt{\frac{\rho_L}{P^*}} \sim 10^{-4}\,\text{s},$$

where $P^* \sim 1$ MPa is the characteristic pressure.

τ_{PP} is much less than the characteristic times of the flow. Thus the pressures in the two phases can be considered equal

$$P_L = P_G = P.$$

(iv) Tables of thermophysical properties of water (Vyckalovitch, Rivkin & Alexandrov 1969) show that for temperatures satisfying the condition (12) the following inequality is valid:

$$\rho_G \ll \rho_L.$$

(v) We assume the difference in the velocities of the phases to be much less than the liquid velocity

$$|u_G - u_L| \ll u_L,$$

where u_G is the bubbles velocity, u_L is the liquid velocity. This assumption will be confirmed by numerical modelling.

(vi) We assume that the phase velocity difference variations are much smaller than the velocity variations

$$\left|\frac{\partial u_G}{\partial x} - \frac{\partial u_L}{\partial x}\right| \ll \left|\frac{\partial u_L}{\partial x}\right|.$$

(vii) The equation

$$\rho_L(P, T_L) = \frac{1}{k(T_L) - P/[\beta(T_L)]^2} \tag{18}$$

approximates the state of the water near the saturation curve with great accuracy. It reflects the experimental fact that isotherms for water in a (P–V) diagram are straight lines for pressure variations within the range of 100 bar near the saturation pressure. In (18) β is the coefficient of the isothermic liquid compressibility on the saturation curve for $T_s = T_L$:

$$k(T_L) = \frac{1}{\rho_{Ls}(T_L)} + \frac{P_s(T_L)}{[\beta(T_L)]^2},$$

where $P_s(T_L)$ is the pressure of saturation at T_L; ρ_{Ls} is the liquid density on the line of saturation at T_L.

In modelling adiabatic flows of boiling liquid like ours, the dependence of liquid density on its temperature can be neglected because liquid density variations $\Delta\rho_L$ due to temperature variations ΔT_L are much smaller than the mixture density variations $\Delta\rho$ due to vapourization caused by thermal energy ($c_L \Delta T_L$) release:

$$\Delta\rho_L(\Delta T_L) \ll \Delta\rho(\Delta T_L).$$

The mixture density

$$\rho = \rho_L(1-\epsilon) + \rho_G\epsilon \tag{19}$$

characterizes the properties of the two-phase mixture and its major changes are caused by the variations in volumetric vapour fraction ϵ.

Neglecting the dependence of liquid density on temperature, we used the equation of the liquid state $\rho_L = \rho_L(P, T_L)$ in the following form:

$$\rho_L = \rho_L(P, T_0)$$

where T_0 is the initial temperature of the liquid.

So the equation of state for liquid (18) can be rewritten as

$$\frac{1}{\rho_L} = k - \frac{P}{\beta^2}, \tag{20}$$

where

$$\beta = \beta(T_0) = \text{const}, \qquad k = k(T_0) = \text{const}.$$

The dependence on pressure in (20) is essential for the initial stage of the process only when the vapour content is small and the mixture properties depend on the liquid compressibility.

(viii) The thermophysical properties of water vapour along the saturation line enable us to introduce the linear approximation

$$\rho_G = P_G / a_G^2, \tag{21}$$

within the range of temperatures $450 \leqslant T_s \leqslant 590$ K. The approximation parameter in (21) has the value $a_G^2 = 2 \times 10^5\ \text{m}^2\ \text{s}^{-2}$.

(ix) We adopt the breakup model based on the Weber criterion: bubbles do not breakup while the Weber number We remains less than its critical value We^*, and on reaching We^* breakup takes place instantaneously. The radii of the bubbles originated are defined to ensure that the Weber number remains at the critical value. This is named the equilibrium breakup scheme:

$$\left.\begin{aligned} &\text{if} \quad We < We^*, \quad \frac{\mathrm{d}c}{\mathrm{d}t} = 0, \\ &\text{if} \quad We > We^*, \quad a = \frac{We^* \sigma}{2\rho_G (u_G - u)^2}, \quad c = \frac{\epsilon}{\frac{4}{3}\pi a^3 \rho}. \end{aligned}\right\} \tag{22}$$

The expression for the Weber number was taken in the following form:

$$We = \frac{2a\rho_G (u_G - u)^2}{\sigma}. \tag{23}$$

To obtain it Nigmatulin (1987) assumed that the basic mechanisms for the development of instabilities on spherical surfaces are the same as for plane interphase boundaries.

The rise in amplitude of a harmonic perturbation with wavelength λ arising on a plane interphase boundary is given by the formula (Birkhoff 1960)

$$\delta = \delta_0 \exp[I(\lambda)t],$$

where δ_0 is the amplitude of the initial perturbation,

$$I(\lambda) = \sqrt{\frac{4\pi^2 \rho_L \rho_G (u_G - u_L)^2}{(\rho_L + \rho_G)^2 \lambda^2} - \frac{8\pi^3 \sigma}{(\rho_L + \rho_G)\lambda^3}}. \tag{24}$$

It is seen from (24) that $I(\lambda)$ will be positive ($I > 0$) when the wavelength of a harmonic perturbation is greater than the critical value:

$$\lambda > \frac{2\pi\sigma(\rho_G + \rho_L)}{(u_G - u_L)^2 \rho_L \rho_G}. \tag{25}$$

On the other hand, according to Nigmatulin's scheme, the length of a wave causing bubble breakup cannot exceed its diameter:

$$\lambda \leqslant 2a. \tag{26}$$

Thus we obtain from (25) and (26) the following inequality:

$$We = \frac{2a(u_G - u_L)^2}{\sigma} \frac{\rho_L \rho_G}{\rho_G + \rho_L} > 2\pi, \tag{27}$$

showing that the perturbation of a bubble surface occurs when the Weber number reaches its critical value: $We^* = 2\pi$. Using assumption (iv) ($\rho_G \ll \rho_L$) we obtain from (27) the expression for Weber number (23) adopted in our model.

The ranges of validity of the model are as follows. Homogeneous nucleation is neglected (assumption i); the coefficient of vapour thermal conductivity is considered to be small in comparison with that of the liquid (assumption ii); the vapour density is small (assumption iv); the approximations of the thermophysical properties of water and its vapour presented are suitable only in a quite narrow ranges (assumptions vii and viii). All these assumptions restrict the temperatures range from above and assumption (viii) restricts it from below. Thus, for water the model can be used for temperatures

$$450 \leqslant T \leqslant 590\,\mathrm{K}.$$

The range of pressures is restricted by the approximations of the thermophysical properties of water:

$$1 \leqslant P \leqslant 20\,\mathrm{MPa}.$$

3.2. *Basic equations of the model*

The equations of mass for the liquid and vapour are the following:

$$\frac{\partial[\rho_L(1-\epsilon)]}{\partial t} + \frac{\partial[\rho_L(1-\epsilon)u_L]}{\partial x} = -jn, \tag{28}$$

$$\frac{\partial[\rho_G \epsilon]}{\partial t} + \frac{\partial[\rho_G \epsilon u_G]}{\partial x} = jn, \tag{29}$$

where u_L and u_G are the liquid and vapour velocities; $n = c\rho$ is the number of bubbles per unit mixture volume.

Summing equations (28), (29) we obtain the equation for the mixture mass conservation (1)

$$\frac{\partial \rho}{\partial t} + \frac{\partial}{\partial x}[\rho u] = 0, \tag{30}$$

where ρ is the mixture density (19);

$$u = u_L + \frac{\rho_G \epsilon}{\rho}(u_G - u_L) \tag{31}$$

is the mean-flow velocity.

Equation (29) can be rewritten in the form

$$\frac{\partial[\rho_G \epsilon]}{\partial t} + \left[u\frac{\partial[\rho_G \epsilon]}{\partial x} + (u_G - u)\frac{\partial[\rho_G \epsilon]}{\partial x}\right] + \rho_G \epsilon \left[\frac{\partial u}{\partial x} + \frac{\partial[u_G - u]}{\partial x}\right] = jn. \tag{32}$$

According to assumptions (v) and (vi) the second terms in square brackets in (32) are

much smaller than the first ones and can be neglected. Then, the equation for vapour mass conservation can be finally written as

$$\frac{\partial[\rho_G\epsilon]}{\partial t}+\frac{\partial[\rho_G\epsilon u]}{\partial x}=jn. \tag{33}$$

The equation for the mixture state (7) can be obtained from (28), (33) and the equations for the liquid and vapour states: (20), (21)

$$\frac{1}{a_f^2}\frac{\mathrm{d}P}{\mathrm{d}t}=\frac{\mathrm{d}\rho}{\mathrm{d}t}+J, \tag{34}$$

where a_f is a 'frozen' speed of sound which characterizes the medium compressibility in the absence of heat and mass exchange between phases

$$a_f=1\Bigg/\sqrt{\frac{\rho(1-\epsilon)}{\rho_L a_L^2}+\frac{\rho\epsilon}{P}}\,, \tag{35}$$

and

$$J=jc\rho^2\left(\frac{1}{\rho_G}-\frac{1}{\rho_L}\right); \tag{36}$$

$a_L=\beta/\rho_L$ is the speed of sound in liquid.

Since the difference in phase velocities is small (assumption v) we can neglect its influence on the interphase heat exchange. Then j is determined from the solution of the problem of the thermal growth of a motionless bubble (Scriven 1959), i.e. using equations (9)–(11).

The momentum equations for the liquid and vapour accounting for assumption (x) have the following form:

$$\rho_L(1-\epsilon)\frac{\mathrm{d}_L u_L}{\mathrm{d}t}+\frac{\partial P}{\partial x}=-nf_\Sigma-jn(u_W-u_L), \tag{37}$$

$$\rho_G\tfrac{4}{3}\pi a^3\frac{\mathrm{d}_G u_G}{\mathrm{d}t}=f_\Sigma+j(u_W-u_G), \tag{38}$$

where u_W is the average velocity at the interface at which the phase transition occurs,

$$\frac{\mathrm{d}_L(\ )}{\mathrm{d}t}=\frac{\partial(\ )}{\partial t}+u_L\frac{\partial(\ )}{\partial x},$$

$$\frac{\mathrm{d}_G(\ )}{\mathrm{d}t}=\frac{\partial(\ )}{\partial t}+u_G\frac{\partial(\ )}{\partial x}$$

are the derivatives taken along the trajectories of liquid and bubbles; f_Σ is the sum of forces acting on a bubble due to its interaction with the surrounding liquid:

$$f_\Sigma=f_b+f_m+f_\mu,$$

with buoyancy force

$$f_b=\rho_L\tfrac{4}{3}\pi a^3\frac{\mathrm{d}_L u_L}{\mathrm{d}t}, \tag{39}$$

virtual mass force

$$f_m=f_m^\circ+f_m'=\rho_L\tfrac{2}{3}\pi a^3\left[\frac{\mathrm{d}_L u_L}{\mathrm{d}t}-\frac{\mathrm{d}_G u_G}{\mathrm{d}t}\right]+\frac{\rho_L(u_L-u_G)}{2n}\left[\frac{\mathrm{d}_G\epsilon}{\mathrm{d}t}+\epsilon\frac{\partial u_G}{\partial x}\right], \tag{40}$$

and drag force

$$f_\mu = -\rho_L \frac{c_\mu}{2} \pi a^2 |u_G - u_L|(u_G - u_L). \tag{41}$$

The last term f'_m on the right-hand side of (40) makes our expression for virtual mass force f_m different from that used by Lahey *et al.* (1980) and other authors on bubble flows. We arrived at this expression having solved the problem of single bubble motion in an infinite volume of incompressible inviscid liquid (Appendix A). This term characterizes the change in the virtual mass force due to the growth (collapse) of bubbles. (The growing bubble draws more liquid into motion and is slowed down in contrast to a collapsing bubble which loses part of its virtual mass and accelerates.) To take into account viscous effects the interfacial drag force (41) was added to f_b and f_m.

The expression for the interfacial drag coefficient c_μ is obtained by extrapolating the c_μ-dependences on Reynolds numbers derived by Adamar-Riybchinskii and Moore (Batchelor 1970) up to their intersection:

$$c_\mu = \begin{cases} \dfrac{16}{Re}, & Re \leqslant 10.9 \\ \dfrac{48}{Re}\left(1 - \dfrac{2.2}{\sqrt{Re}}\right), & Re > 10.9, \end{cases} \tag{42}$$

where the bubble Reynolds number is

$$Re = 2a\rho_L \frac{|u - u_G|}{\mu} \tag{43}$$

and μ is the liquid viscosity.

The equation for mixture momentum conservation can be obtained from (37), (38) and the mass conservation equations for liquid and vapour (28), (29):

$$\frac{\partial}{\partial t}[\rho u] + \frac{\partial}{\partial x}[\rho u^2 + P] = -\frac{\partial}{\partial x}\left[\frac{\rho_L \rho_G \epsilon(1-\epsilon)}{\rho}(u_G - u_L)^2\right].$$

Since phase velocities and their derivatives are similar (assumptions v and vi) the term on the right-hand side can be neglected and the equation for mixture momentum can be taken in the form

$$\frac{\partial}{\partial t}[\rho u] + \frac{\partial}{\partial x}[\rho u^2 + P] = 0. \tag{44}$$

The momentum equation for vapour can be simplified, too. The order of magnitude of the term on the left-hand side of equation (38) can be evaluated as

$$\rho_G \tfrac{4}{3}\pi a^3 \frac{\mathrm{d}_G u_G}{\mathrm{d}t} \sim \rho_G 4\pi a^3 W,$$

where W is the characteristic acceleration.

The order of magnitude of the first component of f_Σ is

$$f_b = \rho_L \tfrac{4}{3}\pi a^3 \frac{\mathrm{d}_L u_L}{\mathrm{d}t} \sim \rho_L 4a^3 W.$$

Since $\rho_G \ll \rho_L$ (assumption iv), the term on the left-hand side of (38) can be neglected.

The last term in equation (38) represents an additional force caused by the bubble's mass variation. Using the mass equation (29), it can be transformed into the

following form:

$$j(u_W - u_G) = \frac{u_W - u_L}{n}\left[\frac{\mathrm{d}_G(\rho_G\epsilon)}{\mathrm{d}t} + \rho_G\epsilon\frac{\partial u_G}{\partial x}\right]. \tag{45}$$

It can be compared with the last term in the expression for the virtual mass force (40) representing the additional force caused by the bubble's virtual mass variation:

$$f'_m = \frac{u_L - u_G}{2n}\frac{\rho_L}{\rho_G}\left[\frac{\mathrm{d}_G(\rho_G\epsilon)}{\mathrm{d}t} + \rho_G\epsilon\frac{\partial u_G}{\partial x}\right] - \frac{u_L - u_G}{2n}\frac{\rho_L}{\rho_G}\epsilon\frac{\mathrm{d}\rho_G}{\mathrm{d}t}. \tag{46}$$

The expressions in the square brackets in (45) and (46) are the same, but the coefficient in front of the brackets in (46) is much larger than that in (45):

$$\frac{|u_W - u_G|}{n} \ll \frac{|u_L - u_G|}{2n}\frac{\rho_L}{\rho_G},$$

because $\rho_G \ll \rho_L$ (assumption iv) and $|u_W - u_G| < |u_L - u_G|$. Thus, the force caused by the bubble's mass variation is much less than the force caused by its virtual mass variation for the present flow:

$$j(u_W - u_G) \ll f'_m.$$

Therefore, neglecting the last term on the right-hand side of (38) the equation for bubble motion will take the form

$$f_b + f_m + f_\mu = 0. \tag{47}$$

Using assumption (v) the derivatives along the trajectories of the liquid and bubbles in equations (39), (40) can be replaced by the derivatives along the mean-flow trajectory.

Since the vapour density is much smaller than that of the liquid, $\rho_G \ll \rho_L$ (assumption iv) and the difference in phase velocities is much smaller than the liquid velocity (assumption v) the mean-flow velocity (31) can be considered equal to the liquid velocity for our flow:

$$u = u_L. \tag{48}$$

Following (48) the liquid velocity in (39), (40) can be replaced by the mean-flow velocity. Then the equation for bubble motion (47) can be rewritten as

$$\frac{\mathrm{d}}{\mathrm{d}t}[\epsilon(u_G - u)] = 2\epsilon\frac{\mathrm{d}u}{\mathrm{d}t} - \frac{3c_\mu|u_G - u|}{4a}[\epsilon(u_G - u)]. \tag{49}$$

Energy conservation equation. We have adopted assumption (iii) that all vapour parameters are equal to those on the line of saturation; therefore vapour enthalpy i_G can always be determined from the pressure in the mixture, $i_G = i_G(P)$. Thus there is no necessity to use the differential equation of vapour energy conservation. Therefore our model contains only one energy equation: the equation for conservation of thermal energy of the mixture in the following form:

$$\rho\frac{\mathrm{d}i}{\mathrm{d}t} - \frac{\mathrm{d}P}{\mathrm{d}t} = -n(u_G - u_L)f_\Sigma - \frac{\partial}{\partial x}\left[\frac{\rho_L\rho_G\epsilon(1-\epsilon)}{\rho}(u_G - u_L)(i_G - i_L)\right]. \tag{50}$$

The first term on the right-hand side is the work done by the forces of interfacial interaction. Assumptions (iv), (v) and (vi) allow us to drop the right-hand side of (50), and it then takes the form

$$\frac{\mathrm{d}i}{\mathrm{d}t} - \frac{1}{\rho}\frac{\mathrm{d}P}{\mathrm{d}t} = 0. \tag{51}$$

Thus we have derived a closed set of equations containing the equation for mixture mass (30), momentum (44), energy (51), the equation of state for the mixture (34), the equation for bubble motion (49), and the breakup model (22). The present form of the set combines both the equations for the mixture as a whole and the equations for one of the phases. The advantage of such a form is that in the limiting cases it gives the equations for the simpler models.

The interfacial drag does not allow bubbles of small radii to get over the threshold for breakup, and the phase velocity difference does not influence the flow parameters. Under these conditions the flow can be described by equations (30), (44), (51), and (34) that do not contain terms reflecting the mechanical non-equilibrium of the mixture and are exactly the same as the equations of the model of boiling at a constant number of nucleation centres (Nigmatulin & Soplenkov 1980).

For flows with a relatively large specific interface area and slow pressure variations the phases stay in thermal equilibrium, $T_L = T_G$ as well: changes in pressure give rise to an intensive heat exchange between phases, rapidly bringing the mixture to equilibrium. The equation of state for the mixture takes the form (4), and equation (34) serves only to determine the intensity of evaporation J. The energy equation (51) for the equilibrium mixture is equivalent to the equation (3) for the entropy.

The possibility of reducing the present model to an equilibrium one allows us to expand the limits of its applicability under certain conditions. For example, the model can be used not only for the modelling of the bubble flows with the vapour volumetric fraction

$$0 \leqslant \epsilon \leqslant 0.3,$$

but also for modelling the equilibrium flows with $0.3 \leqslant \epsilon \leqslant 1$.

4. A short note on the numerical method

A numerical method that excluded pulsations was used to solve this problem. The 'slow wave' is a zone with large gradients of parameters. If one calculates such a flow using the usual methods numerical pulsations occur in place of the wave, and in these, as a rule, negative pressures arise terminating further calculations. To supress numerical pulsations 'pseudoviscosity' is usually introduced in the system of equations. But it is impossible to define a coefficient of pseudoviscosity that permits the 'right' picture of the flow to be obtained. With small coefficients the wave, as before, looks like pulsating structure while with large values it can disappear altogether. (The necessary condition for the existence of the 'slow wave' of boiling is the presence of large gradients. By reducing these gradients pseudoviscosity distorts the physical picture of the flow.)

We have developed a method that prevents the onset of numerical pulsations in the calculations (see Appendix B) so that introducing pseudoviscosity is no longer necessary. Only one regulatory parameter remains: the integration step Δx. Now we can obtain a numerical solution with any necessary degree of accuracy: we reduce Δx until the solution obtained differs from the previous one by a certain chosen value. Therefore we can be sure that the numerical solution obtained corresponds to our system of equations.

5. Free parameters of the model

The free parameters of our model are the number of admixtured particles c_0 and the critical value of the Weber number We^*. For the first computation (figure 5, dotted

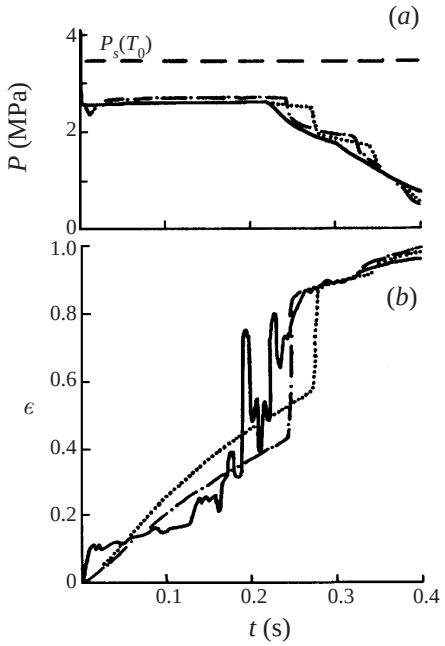

FIGURE 5. The adjustment of the free model parameters. The oscillograms of the pressure (*a*) and volumetric vapour content (*b*) at the cross-section $x = 1.5$ m from the closed tube end: ——, experiment; · · ·, $c_0 = 3 \times 10^5\,\mathrm{kg}^{-1}$ and $We^* = 6$; –·–, $c_0 = 2 \times 10^5\,\mathrm{kg}^{-1}$ and $We^* = 1$.

line) We^* was taken from Nigmatulin's evaluation $We^* = 2\pi \approx 6$; c_0 was chosen as $c_0 = 3 \times 10^5\,\mathrm{kg}^{-1}$) to obtain in the calculations the same pressure level (2.7 MPa) as in the experiment (solid line). The numerical results obtained qualitatively correspond to the experimental ones: the pressure level (2.7 MPa) remains constant for a long time and then suddenly drops; the decrease of pressure is accompanied by the increase in the volumetric vapour content. Thus the 'slow wave' of rarefaction was obtained in the numerical experiments but its velocity was a little less than in the physical experiment.

To achieve a better agreement we decreased the value of We^* and the speed of the 'slow wave' propagation increased. But to maintain the same level of the pressure we had to decrease the number of initial boiling centres at the same time. The results for $We^* = 1$ and $c_0 = 2 \times 10^5\,\mathrm{kg}^{-1}$ are shown by dot-dashed lines in figure 5. Under these initial parameters a better agreement with the experiment was achieved. All the further calculations were carried out using these values of the initial parameters.

Thus varying the free parameters of the model, we obtained good agreement between the 'slow wave' velocity, and the pressures in front of and behind it, and the experimental data. However, while the theoretical and experimental curves coincided in general, the calculated width of the wave was much smaller than that measured in the experiment. The probable reason was the roughness of the 'equilibrium' scheme used for bubble breakup (22). The model described adequately the parameters of the initial and final states of the mixture in the 'slow wave', but gave only a rough estimate for the processes inside it.

Up to now the lack of detailed information on the dynamics of bubble interface instability growth has prevented us from developing a more detailed inertial scheme for bubble breakup. Our model in its present form could be used to describe large-

scale flows with characteristic length scales much larger than the width of the 'slow wave'.

6. Theoretical results and analysis

6.1. *Comparison of experimental and theoretical oscillograms at different tube cross-sections*

A 'slow wave' is clearly seen in figure 1(*c*) where the pressure oscillograms at different tube cross-sections are set out together. Experimental and calculated oscillograms for each of these cross-sections separately are compared in figure 2. It is seen that calculations using the model considering breakup (dash-dot line) correspond with the experiment (solid line) better than those using the model of boiling at a constant number of centres (dotted line) and the equilibrium model (dashed line). The times of arrival of the 'slow wave' are marked A in these oscillograms. On reaching the closed tube end the 'slow wave' is reflected. As a result of the reflection the usual acoustic wave of rarefaction arises which quickly passes through the channel in the opposite direction (from the closed tube end to the exit). The times when it reaches the different cross-sections are marked B. When the second wave of rarefaction reaches the open end the process of efflux is practically finished: all the tube is occupied by a motionless foam (equilibrium media) with a volumetric vapour content $\epsilon \approx 1$.

We see that our model reproduces correctly the main features of the 'slow wave' of rarefaction found experimentally: before its arrival the pressure remains constant for a long time (figure 1); after its arrival the volumetric vapour fraction rapidly increases (figure 2*c*). Now analysing the model and calculations we can establish the mechanism of the 'slow wave'. It is formed a few milliseconds after depressurization at the stage of fast waves.

6.2. *The primary stage of depressurization*

At time zero the pressure at the right-hand end of the 4 m length tube instantaneously drops to atmospheric, 0.1 MPa, and the wave of rarefaction goes deep into the channel with the speed of $1100\,\mathrm{m\,s^{-1}}$. The distributions of parameters along the tube 1, 2 and 3 ms after the vessel is opened are shown in figure 6(*a*). After the arrival of the fast wave of rarefaction the pressure drops below the pressure of saturation and the liquid starts to boil at the existing boiling centres. The boiling causes the expansion of the mixture and thus the flow velocity u behind the wave increases along the channel. Simultaneously, boiling causes the decrease of the speed of sound. And the regime of 'choking' characterized by the equality of velocities of the flow and sound at the exit

$$u(x = 4\,\mathrm{m}) = a_f$$

is reached quickly in the channel (figure 6*b*). In this regime the low atmospheric pressure can no longer penetrate into the channel. The pressure behind the wave is set at the level of 2–2.5 MPa which is less than the pressure of saturation, 3.5 MPa. Also, the 'choking' of the flow leads to the establishing of a large pressure gradient at the exit. The sizes of bubbles are also maximal here. Therefore the Weber number reaches its critical value at the channel exit first. Bubble breakup begins there (figure 6*c*) and the 'slow wave' is being formed.

Our model predicts a higher pressure near the exit than that predicted by the model with no breakup (figure 3). Our prediction corresponds better to the experiment (circles in figure 3).

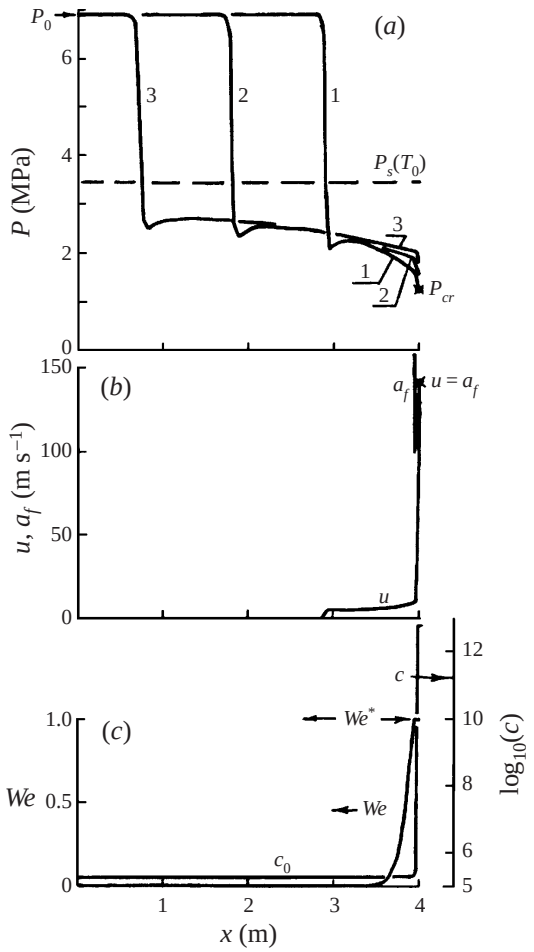

FIGURE 6. The propagation of the first wave of rarefaction through the channel. (*a*) The pressure distribution along the channel after 1, 2 and 3 ms. (*b*, *c*) The distribution of other parameters at $t = 1$ ms.

At $t = 3.6$ ms the fast wave of rarefaction reaches the closed tube end and is reflected from it. A reflected wave of rarefaction forms, moving away from the closed end (figure 7). It propagates through the boiling mixture with the pressure 2.5 MPa. The pressure behind the wave is much less, ≈ 1 MPa. The temperature of saturation corresponding to this pressure is $T_s \approx 450$ K (the overheats are ≈ 60 K). Such enormous overheats cause intensive liquid boiling. The volumetric vapour fraction near the closed tube end increases quickly (figure 7*b*). Since the mixture pressed against the closed tube end has no possibility of expanding, the increase in volumetric vapour fraction causes a pressure increase. As a result, the reflected wave damps quickly and by time $t = 10$ ms (figure 8) a uniform pressure distribution is settled along the whole channel except for a small zone near its exit where the 'slow wave' had formed by that time.

Then the main stage of the efflux process begins. The picture of the flow is very simple (figure 9*a*): a 'slow wave' of rarefaction with velocity ≈ 10 m s^{-1} moves through the zone of nearly constant pressure.

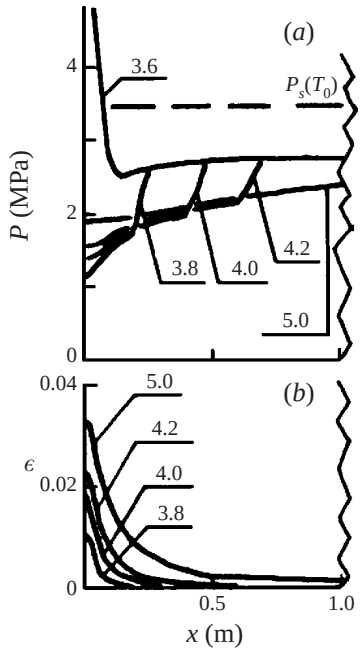

FIGURE 7. The reflection of the fast wave of rarefaction from the closed tube end. The distributions of the pressure and volumetric vapour content at different times, shown in milliseconds.

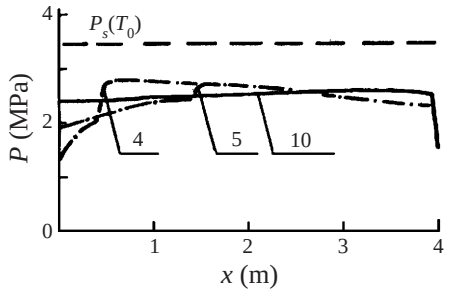

FIGURE 8. The end of the stage of fast waves: the damping of the reflected wave. The pressure distribution at three times, shown in milliseconds.

6.3. *The main stage of efflux*

The parameter distributions along the channel 0.1, 0.2 and 0.3 s after the depressurization are shown in figure 9. Three zones are clearly distinguished in the flow: a non-equilibrium zone, where the liquid and vapour temperatures differ; a 'slow wave' which is a relatively thin moving zone where, nevertheless, most of the vapour is generated and the non-equilibrium mixture is transformed into an equilibrium one; and an equilibrium boiling zone. Let us consider these zones separately.

(i) The non-equilibrium zone is located between the closed tube end and the front of the 'slow wave' (figure 9*a*). Liquid boils only at initial centres in this zone (figure 9*h*). The pressure gradients are very small and the pressure appears constant but, nevertheless, the mixture moves. This movement is caused by non-equilibrium boiling. Since the pressure is less than the pressure of saturation the bubbles are growing and the mixture expands. The expanding mixture is pushed away from the closed tube end.

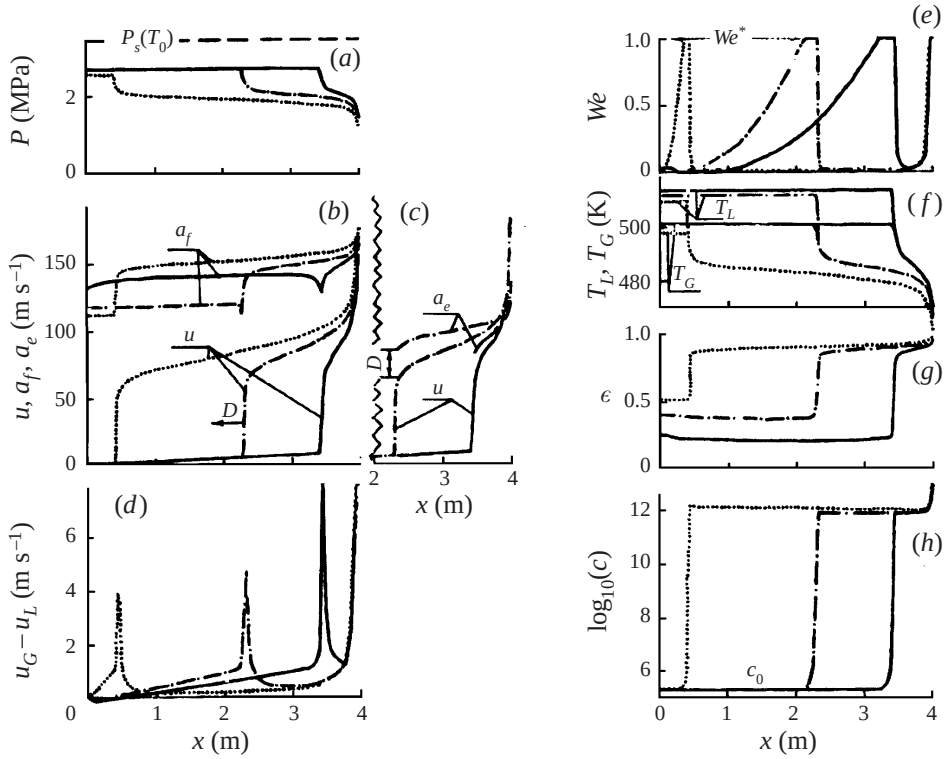

FIGURE 9. The stage of the 'slow wave'. The distribution of parameters along the channel at 0.1 (——), 0.2 (–·–) and 0.3 (···) s.

Since the concentration of boiling centres and the liquid overheats are uniform along the zone the intensity of mixture expansion is also uniform. Therefore the mixture velocity along the zone increases by a linear law (figure 9*b*) from 0 to $u_{max} \approx 10\,\mathrm{m\,s^{-1}}$. The mixture accelerates: in the time taken for a particle to pass through this first zone $\tau_1 \sim L_1/u_{max} \sim 0.1\,\mathrm{s}$ its velocity increases to u_{max}. Thus the acceleration is

$$\frac{\mathrm{d}u}{\mathrm{d}t} \sim \frac{u_{max}}{\tau_1} \sim 100\,\mathrm{m\,s^{-2}}.$$

To create such an acceleration the pressure difference between the ends of the first zone must be only $\sim 0.1\,\mathrm{MPa}$. Since the pressure level in this zone is $\approx 3\,\mathrm{MPa}$ such a small change can hardly be distinguished in figure 9(*a*).

However, the flow acceleration in the first zone is 10 times greater than the gravitational acceleration. The bubbles move faster than the surrounding liquid in accelerated flows, and the acceleration of $100\,\mathrm{m\,s^{-2}}$ proves to be sufficient to increase the phase velocity difference up to $\sim 1\,\mathrm{m\,s^{-1}}$ (figure 9*d*). For such a difference the Weber number (for a 1 mm bubble) reaches its critical value (figure 9*e*) and the bubble surface loses its stability. The cross-section where the Weber number becomes critical is the boundary of the first zone.

Thus, in the first zone the mixture is being prepared for bubble breakup. The processes in this zone determine the velocity of its boundary (the velocity of the 'slow wave'). From the other side, the level of pressure in this zone is defined by the processes taking place in the other zones.

(ii) The second zone contains the 'slow wave' of rarefaction, i.e. a moving zone of sharp parameter changes. Although it is only $\frac{1}{100}$ of the total channel length, most of the liquid is evaporated in this zone. The volumetric vapour content increases from ≈ 0.2 to 0.8 (figure 9*g*). The mixture in the zone is converted into an equilibrium state: liquid and vapour temperatures become equal $T_L = T_G$ (figure 9*f*). Such an intensification of boiling is possible due to the great increase in the interphase area caused by bubble breakup. The number of bubbles in this zone increases by 6 orders of magnitude (figure 9*h*).

(iii) The third, equilibrium, zone is located between the 'slow wave' and the open end. Calculations show that liquid and vapour temperatures are equal, $T_L = T_G$, in this zone (figure 9*f*). The mechanical properties of such a medium are similar to those of gas but with a more complex equation of state (4).

6.4. *The mechanism of the 'slow wave'*

Let us analyse the mechanism that permits practically instantaneous evaporation of such a great quantity of liquid.

The numerical calculations showed that the width of the 'slow wave' is small and does not increase in time. That allows us to suppose that the 'slow wave' can be described by stationary equations in the coordinate system linked with the wave. To test this hypothesis we consider the stationary version of our model:

$$G = \rho v = \text{const}, \tag{52}$$

$$R = Gv + P = \text{const}, \tag{53}$$

$$I = i + \frac{v^2}{2} = \text{const}, \tag{54}$$

$$\frac{\partial v}{\partial y} = \frac{cj\rho(1/\rho_G - 1/\rho_L)}{1 - v^2/a_f^2}, \tag{55}$$

$$\frac{\partial}{\partial y}[\epsilon \Delta v] = 2\epsilon \frac{\partial v}{\partial y} - \frac{3c_\mu |\Delta v|}{4av}[\epsilon\, \Delta v], \tag{56}$$

where y is the distance from the cross-section at which breakup begins, v is the flow velocity in the moving system, and $\Delta v = u_G - u$ is the difference in phase velocities.

All the parameters at $y = 0$ but the velocity v were taken from the numerical experiment: $P = 2.7\,\text{MPa}$, $\epsilon = 0.2$, $T = 513\,\text{K}$, $We = We^*$. The velocity v was varied to see if the solution of a 'shock wave' type could be obtained. This type of solution is characterized by a rapid change of parameters in a narrow zone and relatively small change outside the zone:

$$\frac{\partial v}{\partial y} \to 0, \qquad y \to \infty.$$

The results show (figure 10) that among the integral curves there were such solutions (OA and OB). In those regimes the mixture reached the equilibrium state ($T_G = T_L, j = 0$) and the velocity reached the steady value. In a P–V (pressure–specific volume) coordinate system the states A, B form a segment of the conventional Hugoniot curve with energy release (figure 10*b*) well known from the theory of combustion. The regimes of OC type for which the flow velocity reached the 'frozen' speed of sound a_f could not take place in a 'slow' wave.

In our numerical calculations regime OB appeared because it was a self-sustaining one: the flow velocity behind the wave was equal to the speed of sound in an

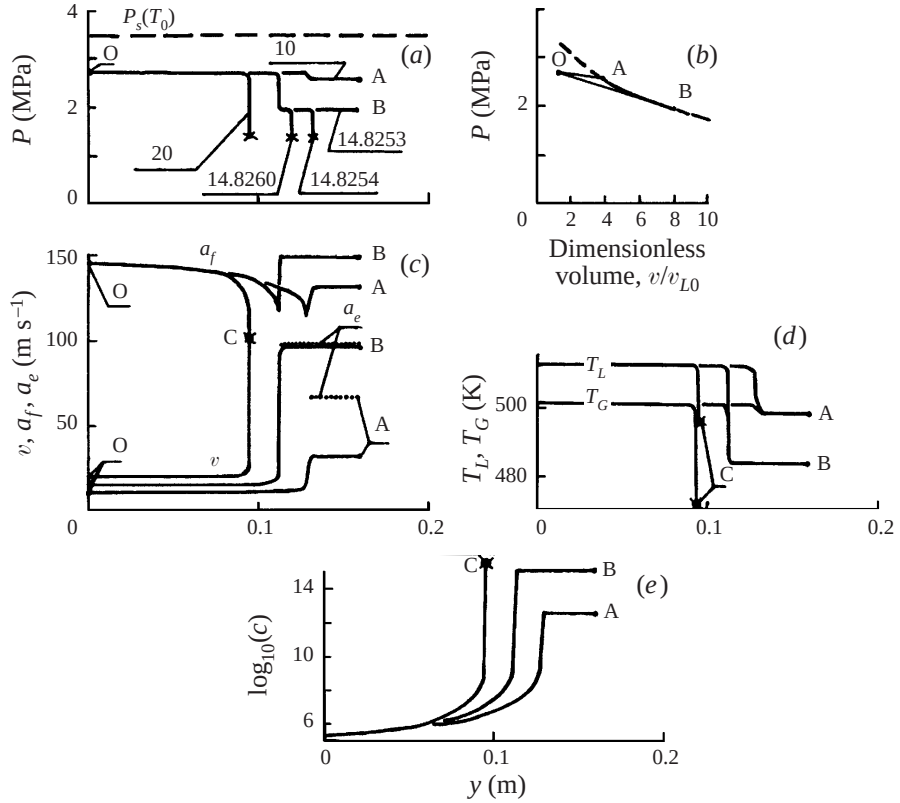

FIGURE 10. The structure of the 'slow wave' calculated using stationary equations. The curves correspond to different values of the flow velocity in front of the wave (the velocity values are shown in m s^{-1} in *a*). (*c*, *d*, *e*) The distribution of the other parameters along the channel for three typical regimes OA, OB, OC. (*b*) The Hugoniot curve with energy release, the dependence of the specific mixture volume on the pressure behind the wave.

equilibrium medium:

$$y \to \infty, \qquad v = a_e \tag{57}$$

and flow disturbances from the exit could not overtake the 'slow wave' and influence its propagation regime (see figure 9*c* paying attention to the fact that $v = u + D$, where D is the velocity of the wave).

Thus, the slow wave was proved to be a shock-type wave and stationary equations allowed its mechanism to be determined.

The mechanism of the 'slow wave' is the following. At the starting point of the wave ($y = 0$) the Weber number reaches its critical value and the bubbles begin to break up. Due to breakup the interphase area increases and boiling intensifies. The speed of the flow increases (since c is in the numerator of (55)). The increase in velocity gradient $\partial v/\partial y$ causes an increase in the difference in phase velocities Δv (see (56)). The increase in Δv is why the Weber number does not decrease after breakup in spite of the diminishing of bubble radius and so breakup is repeated. Thus, it proceeds like a chain reaction, i.e. one breakup creates the conditions for the next one. That leads to the great increase in bubble number. The breakup process comes to an end when the mixture reaches an equilibrium state ($T_L = T_G$). Then $j \to 0$, $\partial v/\partial y \to 0$ and the chain reaction is switched off.

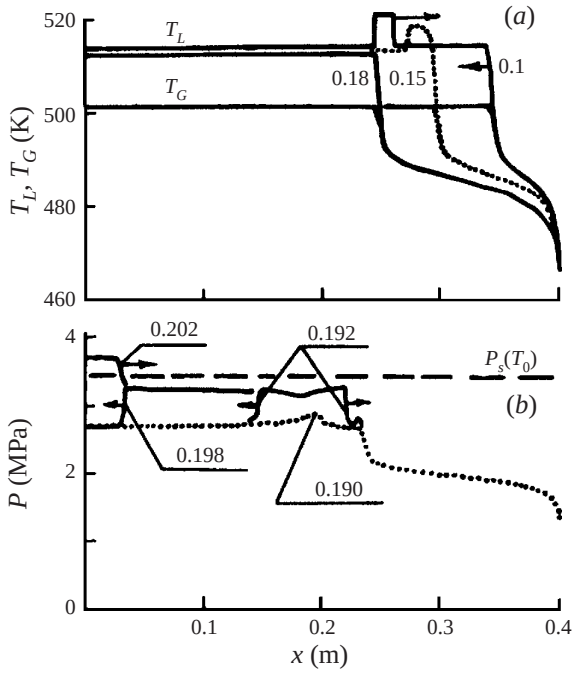

FIGURE 11. Detonation. (*a*) The absorption of the heated layer by a 'slow wave'. (*b*) Conversion of a 'slow wave' into the 'detonation' wave. Numbers in the plot show the time in seconds.

Thus the bubble breakup is the trigger mechanism for the release of the thermal energy of a superheated liquid and its transformation into the kinetic energy of the flow.

7. 'Detonation' in fast flows of boiling liquid

It has been shown that the 'slow wave' of boiling is a self-sustaining wave where the thermal energy of a superheated liquid is transformed into the kinetic energy of fluid–vapour mixture. Thus it has much in common with the deflagration wave in combustion theory where the chemical energy of the metastable combustible mixture is transformed into kinetic energy of the expanding reaction products. It is a rarefaction wave too.

The theory of waves with energy release shows that combustion processes can take place not only in the form of deflagration but also in the form of detonation waves (Smirnov & Zverev 1992). The detonation wave can propagate in a self-sustaining mode as well and represents a stationary structure containing a shock wave followed by a deflagration one. In general the detonation wave is compressive.

Therefore it is reasonable to expect the existence of a 'fast wave of boiling' of compression type propagating with a supersonic velocity. To obtain this wave in the numerical experiment we changed slightly the initial conditions of the problem. We assumed a thin 10 cm length layer in the centre of the channel to be heated up to 525 K, 10 K higher than the liquid temperature in the rest of the tube. The calculations showed that the existence of the hot layer practically did not influence the stage of fast waves and 'slow wave' formation. But at $t = 0.2$ s when the 'slow wave' came in contact with the hot layer (figure 11*a*) the pressure at their point of contact increased

and a compression wave arose. Moving deep into the channel with a sufficiently great speed $D = 200\,\mathrm{m\,s^{-1}}$ the compression wave caused bubble breakup and the mixture conversion into an equilibrium state. As a result of the 'heat explosion' the pressure in the channel doubled.

Along with the 'fast boiling wave' of detonation type moving through the metastable medium a shock wave of retonation type was originated, travelling in the opposite direction towards the exit (figure 11*b*). This wave degenerated very quickly. The process taken as a whole had much in common with the well known deflagration to detonation transition processes (Smirnov & Zverev 1992)

The possibility of the transition of the 'slow waves of boiling' into the detonation mode could be the reason for the high-frequency oscillations observed in non-equilibrium flows of boiling liquid. In fact, any strong disturbance of such flows can intensify the bubble breakup and lead to the formation of a 'fast boiling wave' of detonation type. This wave converts the thermal energy of a superheated fluid into potential energy of the compressed equilibrium mixture, i.e. increasing the pressure. Some of the energy of the wave can be consumed by construction elements (pipelines, dampers, constrictions, etc.) and then partially returned back to the non-equilibrium flow after the induction delay of the structural response. On being returned to the flow it can cause a new strong disturbance resulting in the formation of a new 'detonation boiling wave'. Thus a regime with strong pulsations can be established.

8. Summary and conclusions

1. A model for unsteady processes in boiling liquid was suggested. Using this model the 'slow waves' of boiling appearing in high-pressure-vessel depressurization were explained. We showed that in a 'slow wave' a chain reaction of bubble breakup took place. It caused a sharp increase in the interphase area which led to a sharp intensification of the vaporization process. Thus the non-equilibrium mixture was practically instantaneously transformed into an equilibrium one.

2. It was proved that both 'slow waves of boiling' of deflagration type and 'quick waves of boiling' of detonation type were possible in the non-equilibrium boiling flows. Those waves were shown to propagate in a self-sustaining regime, insensitive to flow disturbances behind the wave.

The following qualitative (energy-based) picture can help to understand the factors causing the origination of these waves in a non-equilibrium boiling mixture. Since the liquid temperature is higher than that of saturation, the liquid in a non-equilibrium mixture is a source of thermal energy. But the small interphase area does not allow the liquid to lose its thermal energy quickly. A sharp increase of the interphase area due to the chain process of bubble breakup makes the liquid lose its thermal energy practically instantaneously. This energy is transformed in the 'slow wave of boiling' into the kinetic energy of the flow. The 'fast wave of boiling' of detonation type transforms the thermal energy into the potential energy of the compressed two-phase mixture.

3. The possibility of strong pulsations due to the periodical formation of the 'fast boiling waves' of detonation type should be taken into account when constructing devices wherein the non-equilibrium flows of boiling liquid can take place.

The Russian Foundation for Basic Research (Grant 99-03-32042) and INTAS (Grant 97-2027) are acknowledged for financial support.

Appendix A. The solution of the problem of bubble movement

A.1. *Physical statement of the problem*

Let a bubble move in an infinite volume of inviscid ($\mu = 0$) incompressible (ρ_L =const) liquid. The direction of the bubble velocity $\boldsymbol{u}_G$ coincides with the direction of the liquid velocity at infinity $\boldsymbol{u}_{L\infty}$. The velocities $u_G, u_{L\infty}$ and the bubble radius change in time:

$$u_G = u_G(t), \quad u_{L\infty} = u_{L\infty}(t), \quad a = a(t).$$

Let us determine the force acting on the bubble.

A.2. *Mathematical statement of the problem*

The flow of inviscid incompressible liquid is described by a Laplace equation that has the following form for axisymmetrical flows:

$$\frac{\partial}{\partial r}\left(r^2\frac{\partial \varphi}{\partial r}\right) + \frac{1}{\sin\theta}\frac{\partial}{\partial \theta}\left(\sin\theta\frac{\partial \varphi}{\partial \theta}\right) = 0, \tag{A 1}$$

where r and θ are the polar radius and angle of a spherical coordinate system with its centre at the bubble centre; φ is the potential of the liquid flow,

$$\nabla(\varphi) = \boldsymbol{v}(r, \theta, t), \tag{A 2}$$

where $\boldsymbol{v}$ is the liquid velocity.

The boundary conditions. The liquid velocity at infinity is

$$r \to \infty, \qquad \nabla(\varphi) = \boldsymbol{i}u_{L\infty}, \tag{A 3}$$

where $\boldsymbol{i} = \boldsymbol{\epsilon}_r\cos(\theta) - \boldsymbol{\epsilon}_\theta\sin(\theta)$ is a unit vector of the axis $0x$ the direction of which coincides with the direction of bubble movement, vectors $\boldsymbol{i}, \boldsymbol{u}_{L\infty}, \boldsymbol{u}_G$ are collinear; $\boldsymbol{\epsilon}_r, \boldsymbol{\epsilon}_\theta$ are the unit vectors of the spherical coordinate system.

The boundary condition on the bubble surface is a slip condition, that is the normal projections of liquid velocity $\boldsymbol{v}\cdot\boldsymbol{\epsilon}_r = \partial\varphi/\partial r$ and the bubble surface velocity of $(u_G\boldsymbol{i} + \dot{a}\boldsymbol{\epsilon}_r)\cdot\boldsymbol{\epsilon}_r$ are equal:

$$r = a, \qquad \partial\varphi/\partial r = u_G\cos(\theta) + \dot{a}. \tag{A 4}$$

A.3. *Solution*

We found the problem solution in the form of a sum of standard solutions of the Laplace equation (A 1): the potential of a straight-line flow and the potentials of the source and dipole with their centres at the centre of the bubble. The free parameters of these standard solutions are chosen to satisfy the boundary conditions (A 3) and (A 4). The final formula for the potential has the following form:

$$\varphi = u_{L\infty}r\cos(\theta) - \frac{(u_G - u_{L\infty})a^3}{2r^2}\cos(\theta) - \frac{\dot{a}a^2}{r}. \tag{A 5}$$

The liquid velocity can be determined from (A 5) using (A 2). To determine the pressure distribution we use the momentum equation in the form of a Bernoulli integral:

$$P_a = \Pi(t) - \rho_L\left[\left(\frac{\partial\varphi}{\partial t}\right)_a + \frac{v_a^2}{2}\right], \tag{A 6}$$

where P_a, $\left(\partial\varphi/\partial t\right)_a$, and v_a are the parameters on the bubble surface; $\Pi(t)$ is a function of time only and therefore it does not affect the force we are looking for.

The partial derivative of φ with respect to time in (A 6) is written in the motionless coordinate system, while in the coordinate system moving with the bubble the partial derivative $(\partial\varphi/\partial t)_G$ has the form

$$\left(\frac{\partial\varphi}{\partial t}\right)_G = \frac{\partial\varphi}{\partial t} + \boldsymbol{v}\cdot(u_G\,\boldsymbol{i}). \tag{A 7}$$

Thus equation (A 6) in the moving coordinate system has the form

$$P_a = \Pi(t) - \rho_L\left[\left(\frac{\partial\varphi}{\partial t}\right)_{r=a} - \boldsymbol{v}_a\cdot(u_G\,\boldsymbol{i}) + \frac{v_a^2}{2}\right].$$

Integrating the pressure over the bubble surface

$$f = f_b + f_m = -2\pi a^2\int_0^\pi P_a\cos(\theta)\sin(\theta)\mathrm{d}\theta,$$

we obtain the force

$$f = \rho_L\frac{4\pi a^3}{3}\frac{\mathrm{d}u_{L\infty}}{\mathrm{d}t} - \rho_L\frac{2\pi a^3}{3}\frac{\mathrm{d}(u_G-u_{L\infty})}{\mathrm{d}t} - \frac{\rho_L}{2}(u_G-u_{L\infty})\frac{\mathrm{d}}{\mathrm{d}t}\left(\frac{4\pi a^3}{3}\right). \tag{A 8}$$

Then it can be proved that the mean liquid velocity in the vicinity of the bubble u_L is equal to $u_{L\infty}$. To adapt the formula (A 8) for multiphase flows we should substitute u_L for $u_{L\infty}$.

The radii of bubbles in our flow can change not only due to their growth or collapse but also due to breakup. The breaking process was not taken into account in (A 8) but it is possible in our flow. The formula (A 8) predicts the acceleration of breaking bubbles since the radii diminish. However, it is in contradiction with the physical reality as the total volume of bubbles and, consequently, the total virtual mass does not change under the breaking process. Thus the breakup shoud not lead to bubble acceleration. Formula (A 8) should be modified for those types of flows.

Equation (A 8) could be modified for flows without breakup by subtracting from the right-hand side the equation for the number of bubbles:

$$\frac{1}{n}\left(\frac{\partial n}{\partial t} + u_G\frac{\partial n}{\partial x}\right) + \frac{\partial u_G}{\partial x} = 0 \tag{A 9}$$

multiplied by $2\pi a^3\rho_L(u_G-u_L)/3$. Here n is the number of bubbles per unit mixture volume:

$$n = \frac{\epsilon}{\frac{4}{3}\pi a^3}.$$

Modifying (A 8) one obtains the following formula for the mean force per volume unit:

$$nf = \rho_L\epsilon\frac{\mathrm{d}u_L}{\mathrm{d}t} - \frac{\rho_L}{2}\epsilon\frac{\mathrm{d}(u_G-u_L)}{\mathrm{d}t} - \frac{\rho_L}{2}(u_G-u_L)\frac{\mathrm{d}\epsilon}{\mathrm{d}t} - \frac{\rho_L}{2}\epsilon(u_G-u_L)\frac{\partial u_G}{\partial x}. \tag{A 10}$$

We assume that (A 10) is also valid for the case of bubble breakup since it does not contain parameters that change under the breakup conditions (n or a). Therefore, no additional forces emerge due to breakup, and breaking bubbles do not accelerate.

Appendix B. The numerical method

Consider a simple medium where there exists an analytical solution of the problem of wave propagation. Then it is possible to evaluate the degree of accuracy of the

solutions given by different numerical methods by comparing the numerical results with the exact analytical solution.

The equation of state of the medium is

$$\frac{1}{\rho} = \frac{1}{\rho_0} - \frac{P - P_0}{\beta^2}, \tag{B 1}$$

where β = const, and ρ_0, P_0 are the density and the pressure in an undisturbed medium.

Introduce dimensionless parameters $\overline{P}, \overline{u} \ldots$.

$$\overline{P} = P/P^*, \qquad \overline{u} = u/u^*,$$

where $P^*, u^* \ldots$ are the characteristic values.

Taking the width of the initial disturbance l^* as a characteristic length, the characteristic pressure $P^* = P_0$, the characteristic velocity, density and time are

$$u^* = \frac{P_0}{\beta}, \qquad \rho^* = \frac{P_0}{(u^*)^2}, \qquad \tau^* = \frac{l^*}{u^*}.$$

In a Lagrangian coordinate system dimensionless equations of conservation for mass and momentum and the equation of state are

$$\frac{\partial}{\partial \bar{t}} \left[\frac{1}{\overline{\rho}}\right] = \overline{a} \frac{\partial \overline{u}}{\partial \overline{x}}, \tag{B 2}$$

$$\frac{\partial \overline{u}}{\partial \bar{t}} + \overline{a} \frac{\partial \overline{P}}{\partial \overline{x}} = 0, \tag{B 3}$$

$$\frac{1}{\overline{\rho}} = 1 + \overline{a} - \overline{P}, \tag{B 4}$$

where $\overline{x} = x/l^*$ is the dimensionless Lagrangian coordinate, and $\overline{a} = \beta^2/(\rho_0 P_0)$ is the dimensionless speed of sound.

The system (B 2)–(B 4) has a well known solution of 'progressive wave' type. The initial profiles of waves move along the characteristics

$$\xi = \overline{x} \pm \overline{a}\bar{t} = \text{const}$$

without changing their shape:

$$\overline{P}(\xi) = \text{const}, \qquad \overline{u}(\xi) = \text{const}.$$

Now consider the problem of the wave propagation numerically using the most popular Lax–Wendroff method. Let the width of the wave be $l^* = 1$, and the pressure in it change from $\overline{P} = 1$ down to 0.1 (figure 12).

For (B 2), the two-step numerical Lax–Wendroff scheme (figure 12*a*) becomes

$$\left[\frac{1}{\rho}\right]_{j-1/2}^{i+1/2} = \frac{1}{2}\left(\left[\frac{1}{\overline{\rho}}\right]_{j-1}^{i} + \left[\frac{1}{\overline{\rho}}\right]_{j}^{i}\right) + \frac{\overline{a}}{2}\frac{\Delta t}{\Delta x}(\overline{u}_j^i - u_{j-1}^i),$$

$$\left[\frac{1}{\overline{\rho}}\right]_{j}^{i+1} = \left[\frac{1}{\overline{\rho}}\right]_{j}^{i} + \frac{\overline{a}\Delta t}{\Delta x}\left(\overline{u}_{j+1/2}^{i+1/2} - \overline{u}_{j-1/2}^{i+1/2}\right).$$

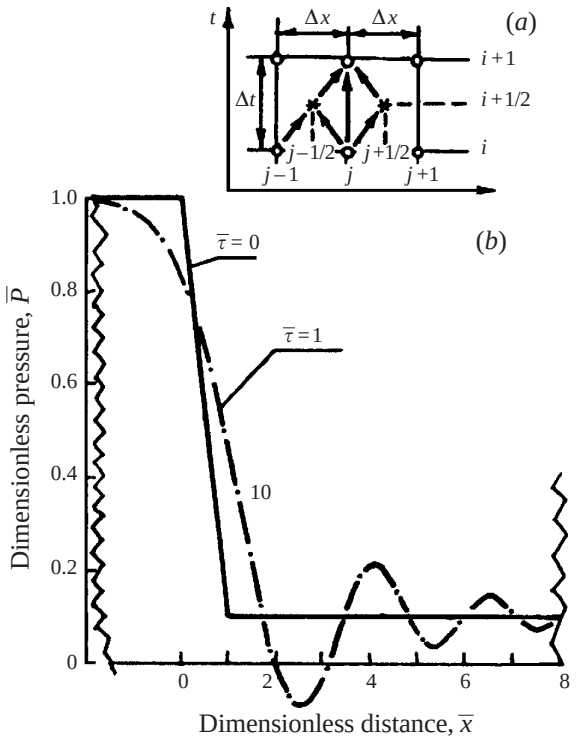

FIGURE 12. (*a*) The Lax–Wendroff scheme. (*b*) According to the analytical solution (——) the wave's shape must not change in the course of time (in the linked coordinate system). Using this analytical solution as initial parameter distributions in a time unit we have obtained a numerical solution (–·–). In this calculation the wave's front was divided into 10 cells.

An analogous numerical scheme can be written for (B 3). The integration steps in time and coordinate satisfy the Courant criterion

$$C = \frac{\bar{a}}{\Delta\bar{x}_0/\Delta\bar{t}} \leqslant 1,$$

where the Courant number C is the ratio of the physical velocity of information spreading and the velocity found using the scheme. We chose $C = 0.5$, divided the front of the wave into 10 cells and added 100 cells from the left and from the right of the wave where according to the analytical solution the parameters should not change. We added one cell on the right boundary and withdrew one cell from the left boundary within each two steps so that the wave should stay in the same place.

The numerical solution proved to differ from the analytical one. In the numerical solution there were 'pulsations' which increased in time (figure 12). Their amplitude was the higher the steeper the wave.

Introducing the pseudoviscosity diffuses the wave and greatly changes the structure of the zone of large gradients. Thus it is unacceptable for modelling the structure of the 'slow boiling wave' as the internal chain process of bubble breakup is the governing process for the whole problem.

To develop a new method satisfying our requirements of being non-oscillatory and preserving the structure of the zones of large gradients we use the physical approach presenting the system of equations (B 2)–(B 4) in the characteristic form where each

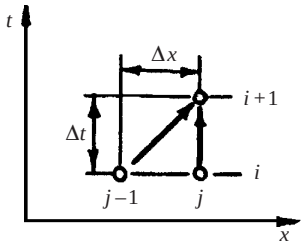

FIGURE 13. The scheme 'triangle'.

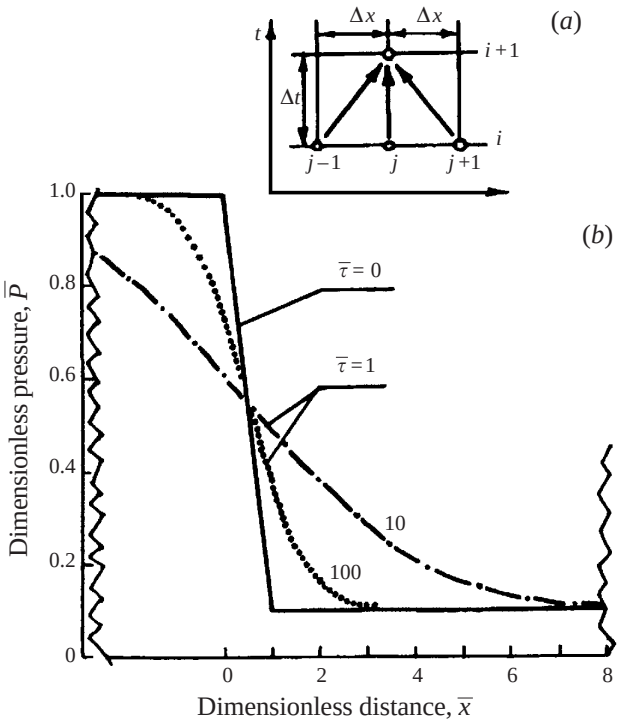

FIGURE 14. (*a*) The scheme 'double triangle'. (*b*) The results of the calculations of the wave structure obtained with this scheme: ——, analytical solution; –·–, numerical solution for 10 cells within the zone of the wave; ···, numerical solutions for 100 cells within the zone of the wave.

equation contains an invariant preserved along the characteristic line:

$$\frac{\partial I_1}{\partial \bar{t}} + \bar{a}\frac{\partial I_1}{\partial \bar{x}} = 0, \tag{B 5}$$

$$\frac{\partial I_2}{\partial \bar{t}} - \bar{a}\frac{\partial I_2}{\partial \bar{x}} = 0, \tag{B 6}$$

where $I_1 = \overline{P} + \bar{u}$; $I_2 = \overline{P} - \bar{u}$ are the invariants. The characteristic directions are given by the equations

$$\frac{\mathrm{d}\bar{x}}{\mathrm{d}\bar{t}} = \bar{a}; \qquad \frac{\mathrm{d}\bar{x}}{\mathrm{d}\bar{t}} = -\bar{a}.$$

Superposition of these two invariants gives us the solution of the problem. Equations (B 5) and (B 6) are independent from each other: (B 5) describes the propagation of perturbations moving from left to right, (B 6) those in the opposite direction. We use these characteristic features of the system to construct the numerical scheme. We know that scheme 'triangle' (figure 13) is free from the pulsations. And we apply the scheme 'left triangle' for (B 5) and 'right triangle' for (B 6):

$$\left.\begin{aligned}(I_1)_j^{i+1} &= (I_1)_j^i + \frac{\bar{a}\Delta t}{\Delta x}\left[(I_1)_{j-1}^i - (I_1)_j^i\right],\\ (I_2)_j^{i+1} &= (I_2)_j^i + \frac{\bar{a}\Delta t}{\Delta x}\left[(I_1)_{j+1}^i - (I_2)_j^i\right].\end{aligned}\right\} \tag{B 7}$$

On substituting the expressions for the invariants into (B 7) the formulas for $\overline{P}$ and $\bar{u}$ can be obtained:

$$\left.\begin{aligned}\overline{P}_j^{\,i+1} &= \overline{P}_j^{\,i} + \frac{\bar{a}\Delta t}{2\Delta x}\left(\bar{u}_{j-1}^i - \bar{u}_{j+1}^i\right) + \frac{\bar{a}\Delta t}{2\Delta x}\left(\overline{P}_{j-1}^{\,i} - 2\overline{P}_j^{\,i} + \overline{P}_{j+1}^{\,i}\right),\\ \bar{u}_j^{i+1} &= \bar{u}_j^{i+} \frac{\bar{a}\Delta t}{2\Delta x}\left(\overline{P}_{j-1}^{\,i} - \overline{P}_{j+1}^{\,i}\right) + \frac{\bar{a}\Delta t}{2\Delta x}\left(\bar{u}_{j-1}^i - 2\bar{u}_j^i + \bar{u}_{j+1}^i\right).\end{aligned}\right\} \tag{B 8}$$

We solved our problem of progressive wave propagation with the help of this numerical scheme ('double triangle'). We chose the same Courant number $C = 0.5$ to compare the results. It is seen (figure 14) that though the numerical solution differs from the analytical one the distortions no longer have the character of 'pulsations'. The degree of distortion was considerably decreased when the front of the wave was divided into a greater number of cells (figure 14*b*).

We applied the same approach to the solution of the main problem. The governing system of equations was rewritten in the characteristic form and the scheme 'triangle' was applied for each of the characteristic equations. That allowed us to get rid of numerical pulsations in this case as well, and the use of pseudoviscosity was no longer necessary. Thus the numerical method allowed one to approach the exact solution with the required accuracy merely by decreasing the step of integration Δx.

REFERENCES

Birkhoff, G. 1960 *Hydrodynamics*. Princeton University Press.

Batchelor, G. K. 1970 *An Introduction to Fluid Dynamics*. Cambridge University Press.

Edwards, A. R. & O'Brien, T. P. 1970 Studies on phenomena connected with the depressurization of water reactors. *J. Brit. Nucl. Engng Soc.* **9**, 125–135.

Isaev, O. A. 1980 Liquid boiling under a fast pressure fall in an adiabatic unsteady stream. Author's essay of candidate dissertation, Sverdlovsk.

Labuntsov, D. A. & Avdeev, A. A. 1981 Theory of boiling discontinuity. *Teplofizika Vysokikh Temperatur* **V.19**, N.3, 552–556.

Labuntsov, D. A., Kolchygin, B. A., Zacharova, E. A. & Vladimirova, L. N. 1964 The study of bubble growth under the boiling of saturated water in a wide range of pressure changes with the help of rapid filming. *Teplofizika Vysokikh Temperatur* **2**, 446–453.

Lahey, R. T. Jr., Cheng, L. Y., Drew, D. A. & Flaherty, J. E. 1980 The effect of virtual mass on the numerical stability of accelerating two-phase flows. *Intl J. Multiphase Flow* **5**, 281–294.

Nigmatulin, R. I. 1987 *Dynamics of Multiphase Media*, Parts I, II. Nauka, Moscow.

Nigmatulin, B. I. & Soplenkov, K. I. 1980 The study of an unsteady efflux of boiling liquid from channels in a thermodynamic non-equilibrium approximation. *Teplofizika Vysokikh Temperatur* **18**, 118–131.

Scripov, V. P. 1972 *Metastable Liquid*. Nauka, Moscow.

Scriven, L. E. 1959 On the dynamics of phase growth. *Chem. Engng Sci.* **10**, 1–13.

Smirnov, N. N. & Zverev, I. N. 1992 *Heterogeneous Combustion*. Moscow University Press.

Vyckalovitch, M. P., Rivkin, C. L. & Alexandrov, A. A. 1969 *The Tables of Heatphysical Properties of Water and Water Vapour*. Isdatelstvo Standartov, Moscow.

Winters, W. S. Jr & Merte, H. Jr 1979 Experiments and nonequilibrium analysis of pipe blowdown. *Nucl. Sci. Engng* **69**, 411–429.